ELSEVIER

Tectonophysics 343 (2001) 93–109

TECTONOPHYSICS

www.elsevier.com/locate/tecto

Role of magma pressure, tectonic stress and crystallization progress in the emplacement of syntectonic granites. The A-type Estrela Granite Complex (Carajás Mineral Province, Brazil)

C.E.M. Barros [a,b], P. Barbey [a,*], A.M. Boullier [c]

[a] *CRPG-CNRS, UPR 2300, 15 rue N.D. des Pauvres, B.P. 20, 54501 Vandoeuvre-lès-Nancy Cedex, France*
[b] *Departamento de Geoquímica e Petrologia, Universidade Federal do Pará, CP 1611, CEP 66075-900, Belém, Brazil*
[c] *LGIT-IRIGM, B.P. 53, F-38041 Grenoble Cedex 9, France*

Received 8 September 2000; accepted 22 October 2001

Abstract

The Archaean, syntectonic, A-type Estrela Granite Complex (Carajás Mineral Province, Brazil) consists of three plutons emplaced in a greenstone sequence under low-pressure conditions ($180 < P < 310$ MPa). It is composed mainly of annite-, ferropargasite (±hedenbergite)- and ilmenite-bearing monzogranites. The contact aureole is affected by a subvertical penetrative schistosity conformable with the limits of the plutons. Meso- to microstructures and mineral reactions in the granites indicate that deformation occurred in a continuum from above-solidus to low-T subsolidus conditions. Two distinct planar structures are observed: (i) a concentrical primary foliation (S_0) corresponding to rhythmic, isomodal, phase layering associated with a faint grain shape fabric; it is horizontal in the centre and vertical towards the edges of the plutons; and (ii) a steep to subvertical foliation (S_1) associated with the deformation of S_0 and accompanied with emplacement of synplutonic dykes and veins of leucocratic granites and pegmatites. Emplacement, differentiation and consolidation of the Estrela Granite Complex are considered to result from a continuous evolution under decreasing temperatures in a single-stage strained crust (transpression), with two main periods. (1) The first period is controlled by body forces, and it corresponds to inflation with magma ponding. As long as the rheology is melt dominated, magma pressure is the critical parameter and almost no strain is recorded. With decreasing T, magmas crystallize and differentiate leading to a concentrical magmatic phase layering. The growing magmatic bodies are mechanically decoupled from the country rocks and their evolution depends on internal magma chamber processes. (2) For higher amount of crystallization (residual melt fraction $F < 0.5$), the role of magma pressure becomes insignificant. Establishment of a continuous crystal framework leads to the coupling of plutons with their surroundings, and deformation in response to tectonic stress. Most of the strain is recorded during this period which starts from the rigid percolation threshold, and extends to subsolidus low-grade conditions. This leads to deformation of the partially crystallized volume and redistribution of fluid-enriched differentiated melts. The amount of crystallization through the rheological thresholds appears as the critical parameter determining the transition from magma-controlled processes (inflation and differentiation of the magma chamber, with development of a phase layering) to tectonic-controlled processes (deformation of the phase layering and redistribution of residual melts). This accounts for the fact that syntectonic plutons commonly display

* Corresponding author. Tel.: +33-83-59-42-34; fax: +33-83-51-17-98.
E-mail address: barbey@crpg.cnrs-nancy.fr (P. Barbey).

PII: S0040-1951(01)00260-8

intermingled, boudinaged layers with distinct modal compositions and in some cases well-preserved rhythmic layering.

Keywords: Brazil; Carajás Mineral Province; Archaean; A-type granites; Syntectonic pluton; Phase layering

1. Introduction

The structural and lithological characteristics of plutons (shape, fabrics, distribution of rock types, etc.) result from a complex history of magma delivery and pluton growth within a dynamic regional context, the whole process being controlled more particularly by the stress field, the magma hydrostatic pressure, the anisotropy of the country rocks and the degree of crystallization.

Magma pressure (P_m) appears as one of the parameters controlling magma transport and emplacement as well as shape of plutons (e.g. Baer and Reches, 1991; Hogan and Gilbert, 1995; Roman-Berdiel et al., 1995; Hutton, 1997; Hogan et al., 1998; Vigneresse et al., 1999). However, the observation that coeval and compositionally similar plutons display different structural patterns led Castro (1987) to suggest that their emplacement conditions are also determined by tectonic factors. It appears now from numerous structural studies, gravity data and analogue modelling that magma ascent and emplacement are controlled by the stress field (see the review by Vigneresse and Clemens, 2000). The dynamics of pluton emplacement being the result of an interplay between internal buoyancy forces and tectonic stresses (e.g. Hutton, 1988, 1997), magma pressure is considered as an indistinguishable part of the regional stress field (concept of magma driving pressure of Hogan et al., 1998). Vigneresse et al. (1999) give a detailed account of the role of magma intrusion on the regional stress field and of implications to the shape of granitic intrusions (see also McCarthy and Thompson, 1988; Parsons et al., 1992). Moreover, in the case of an anisotropic state of stress of the crust, different pluton orientations may be expected (position of tension gashes, elongated plutons with their long axis orthogonal or oblique to the principal stress direction…), depending on the relationships between magma pressure, tensile strength of the crust and differential stress applied to the system (e.g. Wickham, 1987; Davidson et al., 1994; Pons et al., 1995; Gleizes et al., 1997, 1998; Castro and Fernandez, 1998).

The presence of large-scale strength anisotropy of the country rocks is also recognized as a fundamental parameter controlling the level of emplacement of an intrusion (Clemens and Mawer, 1992). This anisotropy may correspond, for instance, to either an unconformity along which magma spreads out (Hogan et al., 1998), or a vertical foliation localizing a tensional shear fracture and leading to permissive magma emplacement and different distributions of lithologies inside the plutons (Castro and Fernandez, 1998).

Experimental data show that silicic melt viscosities cluster at $10^{4.5}$ Pa s irrespective of pre-eruptive conditions (Scaillet et al., 1999, 2000) and, therefore, that granitic plutons result from the aggregation of crystal-poor, low-viscosity magmas, in agreement with fracture-induced magma propagation as a mechanism of magma emplacement at shallow crustal levels (e.g. Vigneresse and Clemens, 2000). The occurrence of rhythmic layering near the margins of many plutons, worldwide, including syntectonic ones (e.g. Balk, 1937; Barrière, 1981; Marre, 1986; Stephenson, 1990; Pons et al., 1995) implies that pluton consolidation involved fractional crystallization (± gravity settling, flow segregation) either within a periodically replenished convecting magma chamber (e.g. Brandeis and Marsh, 1989; Tait and Jaupart, 1996), or by repeated injection related to roof-block subsidence (e.g. Clarke and Clarke, 1998). Moreover, crystallization does not solely control the igneous layering development but also controls the rheology of magmatic bodies through the rheological thresholds (Arzi, 1978; Van der Molen and Paterson, 1979; Vigneresse et al., 1996), resulting in different fabrics (Hutton, 1988; Bouchez et al., 1992).

Nevertheless, despite the apparent structural and lithological complexity of many plutons, their whole emplacement appears to result from a continuous deformation process combined with crystallization and subsolidus cooling (e.g. Paterson et al., 1989;

Miller and Paterson, 1994; Tribe and D'Lemos, 1996; Schofield and D'Lemos, 1998; Althoff et al., 2000), resulting in fabrics likely to reflect internal, crystallization, emplacement and regional processes (Paterson et al., 1998).

This paper intends to discuss how these different processes interact during the emplacement, differentiation and consolidation of syntectonic plutons. Our study is based on an Archaean A-type granite complex from the southeastern part of the Amazonian craton (the Estrela Granite Complex; Barros et al., 1992, 1997). After an overview of the lithology, phase assemblages and relationships of the plutons with the country rocks, (i) we describe their different structures, from magmatic to solid state; and (ii) discuss their evolution in terms of a continuous process within the framework of magma dynamics and pluton growth during a regional deformation event.

2. Geological setting

The Carajás Mineral Province, located SE of the Amazonian craton, is well known for its exceptional mineral deposits (Almeida et al., 1981). A brief description of this province is given below (see Macambira and Lafon, 1995). It comprises the Rio Maria terrain to the south (Althoff et al., 2000), and the Carajás terrain to the north (Souza et al., 1996). The oldest lithologies of the Carajás terrain (Fig. 1) correspond to 3.0-Ga granulites (Pium complex; Hirata et al., 1982; Araújo et al., 1988; Rodrigues et al., 1992) and 2.86-Ga quartzofeldspathic gneisses (Xingu complex; Machado et al., 1991). These formations are overlain by the Grão Pará, Salobo and Pojuca volcano-sedimentary series (Itacaiúnas supergroup) consisting of bimodal volcanics, banded iron formations and rare occurrences of metapelites and calc-silicate rocks (Hirata et al., 1982; Docegeo, 1988). U–Pb zircon dating gives minimum deposition ages of 2760 Ma (Olszewski et al., 1989; Machado et al., 1991), whereas the regional metamorphism occurred under low-grade conditions at 2732 ± 2 Ma (zircon U–Pb; Machado et al., 1991). The Itacaiúnas supergroup is stratigraphically overlain by the Aguas Claras Formation composed of mudstones, siltstones and sandstones (Araújo et al., 1988). It is weakly deformed and recrystallized under very low-grade conditions. Zir-

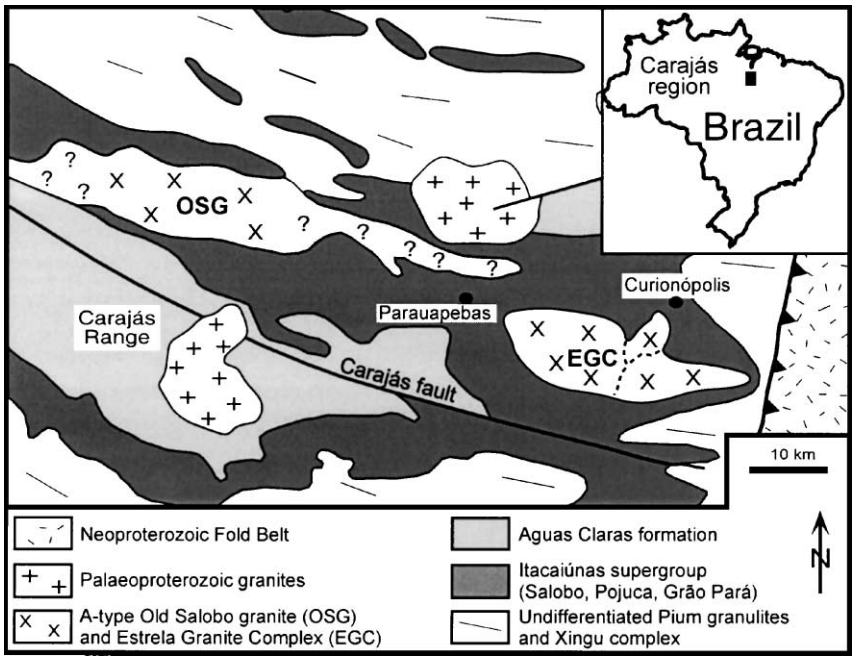

Fig. 1. Geological sketch map of the Carajás terrain (Carajás Mineral Province). Modified from Docegeo (1988) and Araújo et al. (1988).

cons derived from syndepositional volcanism yielded an age of 2681 ± 5 Ma (Trendall et al., 1998), whereas sills and dikes of gabbro and diabase crosscutting the Aguas Claras Formation yielded zircon U–Pb ages of 2708 ± 37 Ma (Mougeot, 1996) and 2645 ± 12 Ma (Dias et al., 1996). The structural evolution of this area is considered to be related to sinistral EW strike–slip movements that led to the deformation of the volcano-sedimentary sequences under low greenschist–facies conditions (Araújo and Maia, 1991; Pinheiro and Holdsworth, 1997).

Several alkaline granite suites intruded either the Xingu Complex or the Itacaiúnas supergroup, as the syntectonic Plaquê Suite emplaced at ca. 2740 Ma (zircon Pb–Pb data; Avelar, 1996; Huhn et al., 1999), the syntectonic Estrela Granite Complex (2763 ± 7 Ma; Pb zircon evaporation data; Barros et al., 2001), the Old Salobo Granite (2573 ± 2 Ma; zircon U–Pb data; Machado et al., 1991) and the Itacaiúnas monzogranite (2560 ± 37 Ma; zircon Pb–Pb data; Souza et al., 1996). The Carajás Mineral Province was later intruded by widespread anorogenic granites at 1.88 Ga (Dall'Agnol et al., 1994).

3. The Estrela Granite Complex

The Estrela Granite Complex appears as an uneven, E–W trending, massif (43 × 15 km) with a stocky western part, a fin-shaped northern extension and a narrow eastern termination (Fig. 2a). This shape, the distribution of granite lithologies and greenstone xen-

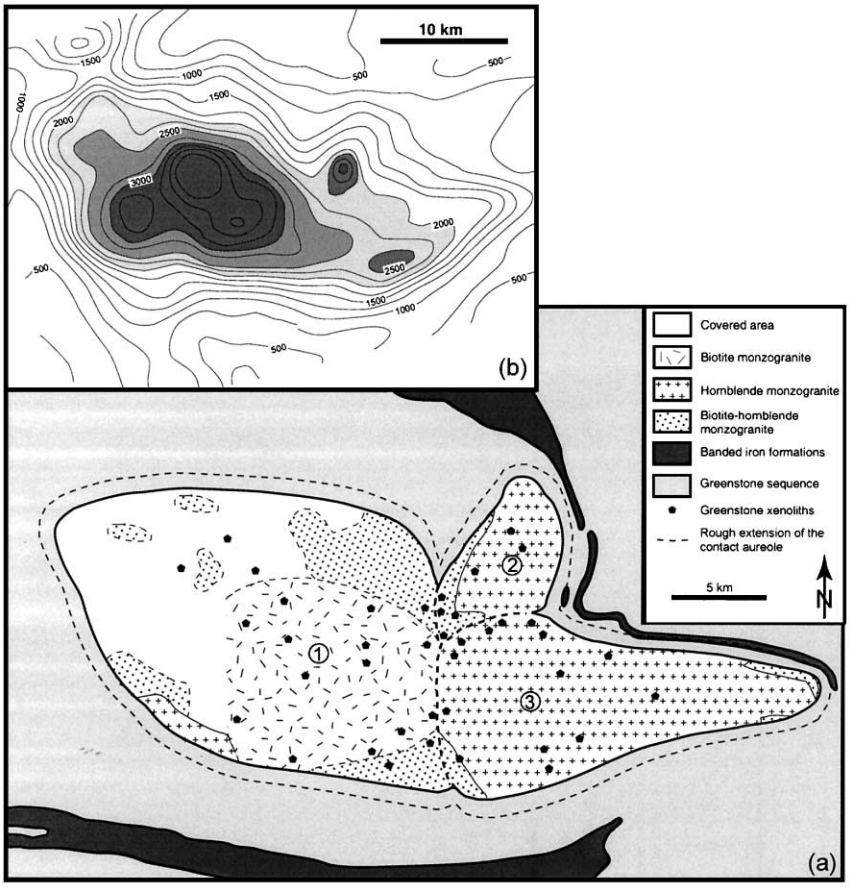

Fig. 2. Lithological (a) and radiometric (b) maps of the Estrela Granite Complex. Radiometric map (total counting) redrawn from Andrade (1991).

oliths, and aeroradiometric data (Fig. 2b) suggest that the Estrela Granite Complex consists of three plutons. This is also supported by structural data showing that the northern extension corresponds to a distinct pluton. Nevertheless, due to discontinuous outcropping conditions, contacts between plutons were not observed and have been deduced from the orientation of the foliation. The Estrela Granite Complex is surrounded by a 1- to 2-km-wide metamorphic contact aureole.

3.1. Rock types

The three plutons of the Estrela Granite Complex consist predominantly of medium-grained, locally porphyritic, metaluminous hornblende–monzogranites, peraluminous biotite–monzogranites and related pegmatites (Table 1 and Fig. 2a). Tonalites, granodiorites and syenogranites are subordinate. Locally at the contact with the country rocks, monzogranites and syenogranites are fine grained. Feldspars consist of microperthitic and perthitic (flame) K-feldspar ($Or_{92-97}Ab_{3-8}An_0$) and of plagioclase (An_{11} to An_{23} with the exception of a few values up to An_{45}). Ferromagnesian minerals consist of annite ($X_{Fe} \geq 0.86$), ferropargasite ($X_{Fe} = 0.79–0.98$; with the exception of tonalites where $X_{Fe} = 0.72$) and hedenbergite ($X_{Fe} = 0.6–0.7$). Accessories are zircon, apatite, ilmenite, allanite and sphene. A study of zircon for U–Pb dating (Barros et al., 2001) shows that it consists of euhedral grains with simple internal structures (limpid magmatic growth zones and occasionally dark, ± metamictic cores). Leucocratic granite, aplite and amphibole-bearing pegmatite occur commonly as late crosscutting dykes. However, the existence of synplutonic bodies is shown for instance by the occurrence of diffuse pegmatite bodies (Fig. 3a), and of deformed pegmatite dykes crosscut by their host granite (Fig. 3b).

The Estrela Granite Complex (Table 1) displays the characteristics of A-type granitoids (Loiselle and Wones, 1979; Collins et al., 1982; Whalen et al., 1987; Eby, 1990, 1992), that is, high $Na_2O + K_2O$ contents (5.7–8.4 wt.%), very high FeO/(FeO + MgO) ratios (0.96–0.99), high amounts of incompatible elements (e.g. Zr = 146–640 ppm, Y = 13–404 ppm, Nb = 21–45 ppm, $\Sigma_{REE} = 350–736$ ppm), moderately fractionated rare-earth patterns [$(La/Sm)_N = 3.09–7.78$; $(Gd/Yb)_N = 1.22–2.33$] and low initial $^{87}Sr/^{86}Sr$ ratios (0.7018 ± 0.002; Barros et al., 1992, 1997).

Table 1
Representative major (wt.%) and trace (ppm) element compositions of the main rock types of the Estrela Complex along with modal compositions (vol.%). Accessories consist of ilmenite, zircon, allanite, apatite and titanite

	Monzogranites				Pegmatite
	Bt	Hbl–Bt	Hbl	Hbl–Cpx	Hbl
SiO_2	72.6	71.5	71.13	72.81	71.64
Al_2O_3	13.06	12.97	13.21	11.80	13.77
Fe_2O_3*	3.91	4.40	3.23	5.71	3.39
MnO	0.02	0.02	0.03	0.06	0.03
MgO	0.24	0.25	0.15	0.05	0.09
CaO	1.18	1.60	2.35	1.95	1.81
Na_2O	3.46	3.21	3.82	3.10	3.54
K_2O	4.21	4.68	3.94	4.07	4.73
TiO_2	0.21	0.25	0.72	0.55	0.23
P_2O_5	0.03	0.04	0.16	0.08	0.08
LOI	0.81	0.78	0.46	0.43	0.47
Total	99.73	99.70	99.20	100.61	99.78
A/CNK	1.1	1.0	0.9	0.9	1.0
X_{Fe}	0.89	0.90	0.91	0.98	0.95
Rb	185	158	144	84	94
Sr	54	60	166	49	151
Nb	29	25	32	29	17
Y	85	74	76	106	48
Zr	292	351	500	545	92
Qtz	27–35	28–40	29–46		10–30
Kfs	20–35	20–37	15–28		30–40
Pl	24–38	20–35	20–30		25–35
Bt	5–20	3–15			
Hbl		2–10	10–20		10–20
Cpx			0–4		

Fe_2O_3* = total iron. LOI = loss on ignition. Mineral abbreviations according to Kretz (1983).
A/CNK = $Al_2O_3/(CaO + Na_2O + K_2O)_{mol}$. $X_{Fe} = Fe/(Fe + Mg)$. Full data set available on request.

3.2. The contact aureole

In the surrounding greenstones far from the granite, magmatic textures are commonly preserved due to a weak, discontinuous regional schistosity. Typical phase assemblages are Act + Chl + Pl ± Bt ± Ep ± Mt ± Qtz in metabasites, and Qtz + Ms + Bt in metapelites, indicative of low-grade regional metamorphic conditions (400 °C < T < 550 °C). Within the contact aur-

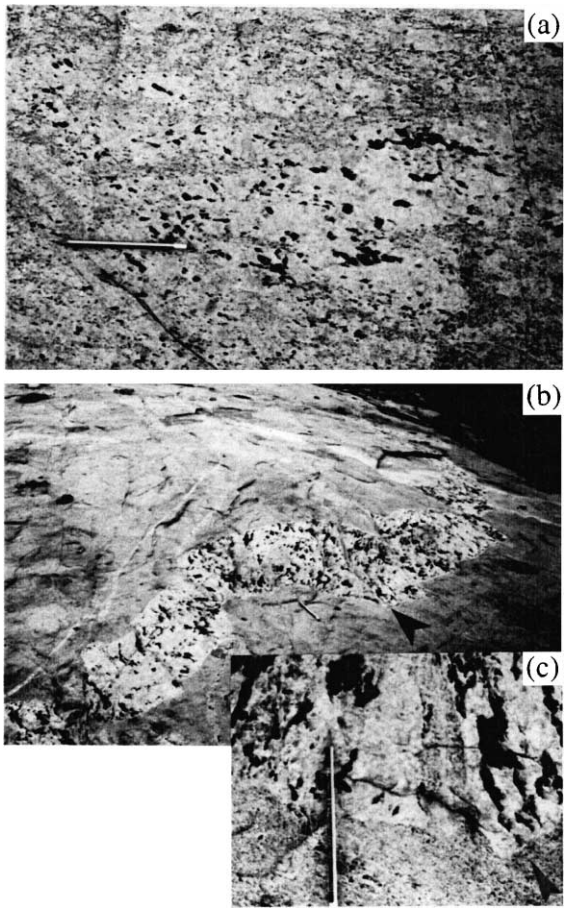

Fig. 3. Hornblende-bearing pegmatites occurring (a) as diffuse bodies, and (b) as syn-plutonic dyke within monzogranite. Inset in (b): close view of the contact showing the host-granite cutting across the dyke. Hornblende crystals are oriented along the S_1 schistosity. Pencil = 15 cm.

eole, the intensity of recrystallization increases towards the granites, the greenstones xenoliths being strongly recrystallized into medium- to coarse-grained granoblastic assemblages. The highest grade contact metamorphic phase assemblages are Hbl + Pl ± Bt ± Hd ± Ilm ± Qtz (metabasites), Hbl + Pl + Bt ± Grt (metagreywackes), and Qtz ± Kfs + Pl + Hd + Spn (calc-silicate rocks). The metabasites are crosscut by decimetre- to metre-long, subvertical, hydrothermal amphibole veins localized within tension gashes or en echelon structures.

In the periphery of the contact aureole, amphibole from metabasites is heterogeneous and consists of an actinolite core surrounded by a hornblende rim, whereas it corresponds to a homogeneous hornblende near the contact with the granite and in the xenoliths. Plagioclase is more limpid and displays more homogeneous compositions in the contact aureole (An_{25-45}) than in the surrounding series (An_{15-75}). A change in phyllosilicate composition is also observed towards the granite as, for instance, an increase in the biotite TiO_2 content (e.g. from 1.8% to 2.8% in metabasites) and in the chlorite X_{Fe} ratio (from 0.2–0.4 to 0.5–0.6).

3.3. Emplacement conditions

Emplacement temperatures were estimated using zircon and apatite saturation thermometry (Watson and Harrison, 1983; Harrison and Watson, 1984). The Zr and P concentrations in biotite– and hornblende–monzogranites (Zr = 146–589 ppm, P = 131–699 ppm, SiO_2 = 69.5–75.1%) yield the following temperatures: 782–893 °C (average: 860 °C) for zircon and 784–929 °C (average: 870 °C) for apatite thermometers. This is consistent (i) with experimental data on the stability field of hedenbergite, ferropargasite and annite suggesting crystallization temperatures of ca. 850 °C (Eugster and Wones, 1962; Gilbert, 1966; Wones and Gilbert, 1982; Kurshakova and Avetisyan, 1974); (ii) with the temperatures for the genesis of A-type granite melts (>900 °C) inferred from experimental data (e.g. Clemens et al., 1986; Creaser et al., 1991; Patiño-Douce, 1997); and (iii) with the abundance of clinopyroxene and the absence of orthopyroxene in mafic xenoliths (see, for instance, Spear, 1993). In the contact aureole, hornblende–garnet assemblages ($XCa_{grt} = 0.09$, $1.16 < \mathrm{Ln}K_D < 1.45$) and biotite–garnet assemblages ($-1.88 < \mathrm{Ln}K_D < -1.62$) yielded temperatures in the 520–610 °C range using the calibrations of Graham and Powell (1984) and Ferry and Spear (1978).

Pressure estimate using Al-in-hornblende barometry is questionable because of very high $Fe^{2+}/Fe^{2+} + Mg$ ratios (0.80–0.98) in the monzogranite amphiboles, far beyond the recommended values (< 0.65 according to Anderson and Smith, 1995). However, an attempt at estimating emplacement pressures was made using amphiboles from the tonalites displaying the lowest $Fe^{2+}/Fe^{2+} + Mg$ ratios (0.72), not too different from the limiting values. The Al_{tot} content of amphibole (1.64–1.66 atom per formula unit) yielded

pressures ranging from 110 MPa for $T = 850$ °C to 380 MPa for $T = 750$ °C with Anderson and Smith (1995) calibration. Although disputable, this estimate is consistent (i) with pressure estimates (180–310 MPa) obtained from actinolite–chlorite pairs ($0.12 < \mathrm{Ln}K_D < 0.25$) from the contact aureole, using the calibration of Laird (1988); and (ii) with the presence of actinolite in association with calcic plagioclase and chlorite (e.g. Kuniyoshi and Liou, 1976).

The stability of ilmenite in the presence of hedenbergite suggests f_{O_2} conditions lower than FMQ + 1 (Wones, 1989). The occurrence of diffuse bodies and synplutonic dykes of pegmatite suggests that magma became fluid saturated towards the end of the course of differentiation. Several mineral transformations occurred during the consolidation of the Estrela Granite Complex, in response to changing T and f_{O_2} conditions (Czamanske and Wones, 1973; Barrière and Cotten, 1979; Wones, 1989), with formation of: (i) ilmenite-bearing quartzofeldspathic pods, (ii) plagioclase–sphene symplectites in deformed monzogranites, (iii) microperthites and flame perthites, and (iv) sphene reaction rims around ilmenite and stilpnomelane-bearing low-grade assemblages. These textures will be discussed further.

4. Structural data

A subvertical foliation (S_c) concordant with the contact of the plutons occurs in the aureole, excepted locally as, for instance, to the northern termination of pluton 2 (Fig. 4a) where a strong subvertical lineation is observed (L-tectonites). At the southern contact of pluton 3, a steep-plunging lineation is associated to S_c, and inclusion trails in syntectonic garnet porphyroblasts indicate a top to the south movement. These structures together with the geometry of the banded iron formations in the surrounding greenstones indicate the synkinematic character of the Estrela Granite Complex.

4.1. Planar and linear fabrics

Planar fabrics identified in all three plutons of the Estrela Granite Complex comprise: (i) a primary magmatic foliation (S_0) with variable attitudes, (ii) a second-formed steep to subvertical foliation (S_1), (iii) local high-temperature mylonitic zones (S_m), and (iv) low-grade closely spaced dissolution joints (S_d) restricted to the contacts.

The primary S_0 foliation is defined by a rhythmic layering corresponding to either the superposition of layers with different proportions of ferromagnesians minerals, or alternating ferromagnesian and quartzofeldspathic layers (Fig. 5a). The superposed layers are isomodal and separated by a phase contact. It should be noticed that S_0 defines a plane of anisotropy along which quartzofeldspathic residual melts may be subsequently injected as veins. These veins, locally abundant, should not be mixed up with the primary igneous layering. S_0 is well preserved in pluton centres where it is horizontal (Fig. 5a). It becomes vertical towards the contacts where it is deformed and hardly distinguished from S_1 (composite S_{0-1} foliation). S_0 is also defined by a grain-shape fabric marked by amphibole, biotite and feldspars. At the microscopic scale, quartz occurs as large grains, locally slightly elongated parallel to S_0. As this primary foliation corresponds basically to an igneous layering, it is likely to result from magmatic differentiation followed by near-solidus solid state deformation.

The S_0 foliation is folded and cut across by a steep to subvertical foliation (S_1), axial planar for the folds. Fold axes display variable, but generally low dips (Fig. 4b), steeply plunging axes being observed locally as a function of the initial position of the S_0 surface. They are close to EW in plutons 1 and 3, and NNE–SSW in pluton 2 (Fig. 4c). S_1 developed in submagmatic to subsolidus conditions. It is locally outlined by synplutonic dykes and veins of leucocratic granites and of amphibole- or biotite-bearing pegmatites and aplites. Veins and dykes parallel to S_1 are rectilinear and display pinch-and-swell structures, whereas those in a position of transversal or diagonal joints, are folded (Fig. 5b and c). Most of the veins display a faint S_1 fabric which is axial planar for folded veins. In pluton 2, the S_0 foliation, subhorizontal or moderately dipping, is crosscut by a steeply-lying, NNE–SSW, S_1 foliation outlined locally by elongated ilmenite-bearing quartzofeldspathic pods (Fig. 6a). A commonly subhorizontal lineation (L_1) is defined by the preferred orientation of amphibole and biotite. It is EW trending in plutons 1 and 3, and NNE–SSW in pluton 2. At the microscopic scale, quartz may be undeformed with a faint preferred

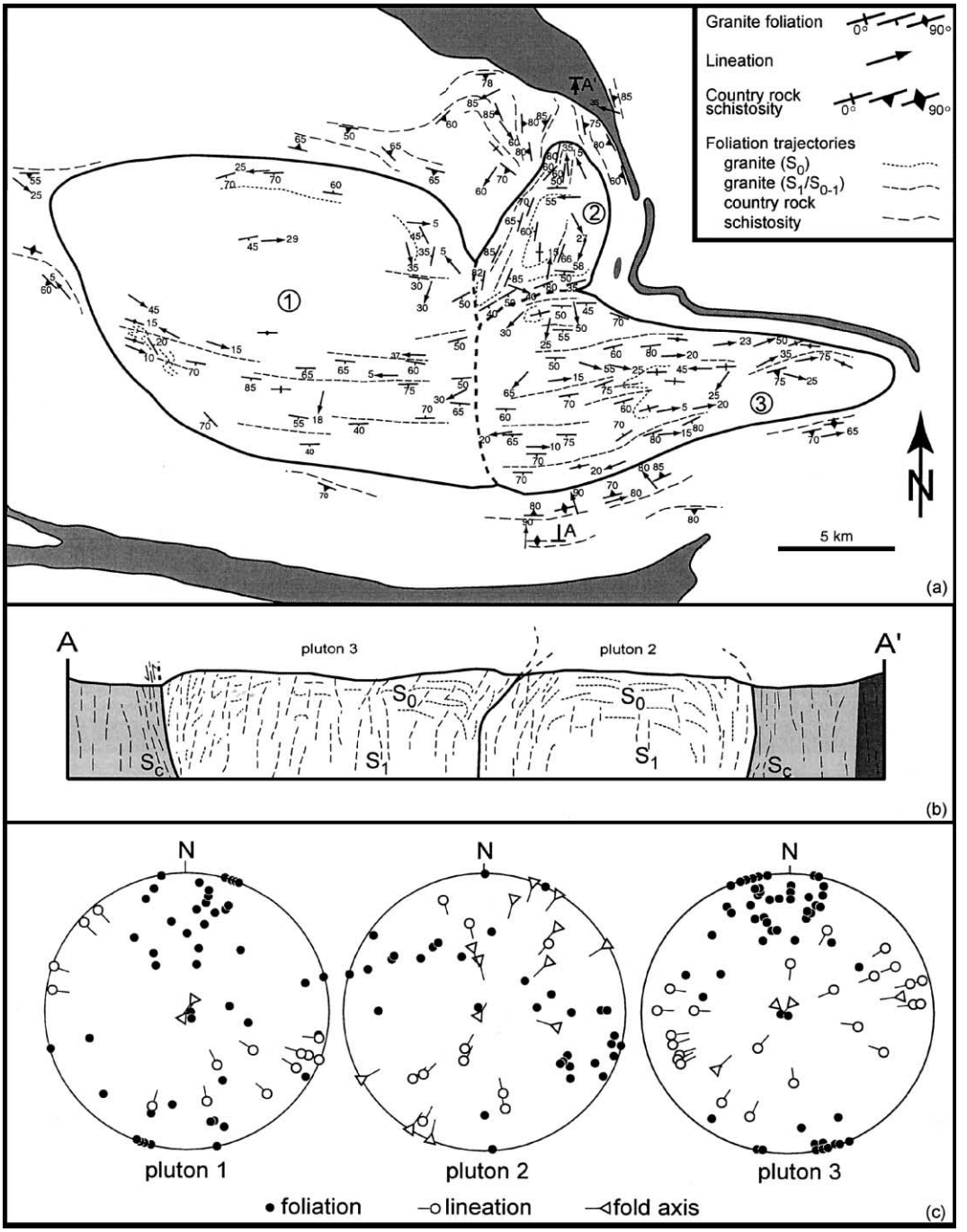

Fig. 4. (a) Structural map of the Estrela Granite Complex, (b) submeridian cross-section through plutons 2 and 3, and (c) stereographic plots for the three plutons. On the structural map, the granite foliation clearly identified as S_0 is shown by dotted lines, whereas the others (S_1 foliation, foliation not clearly identified as S_0 and composite S_{0-1} foliation) are shown by dashed lines.

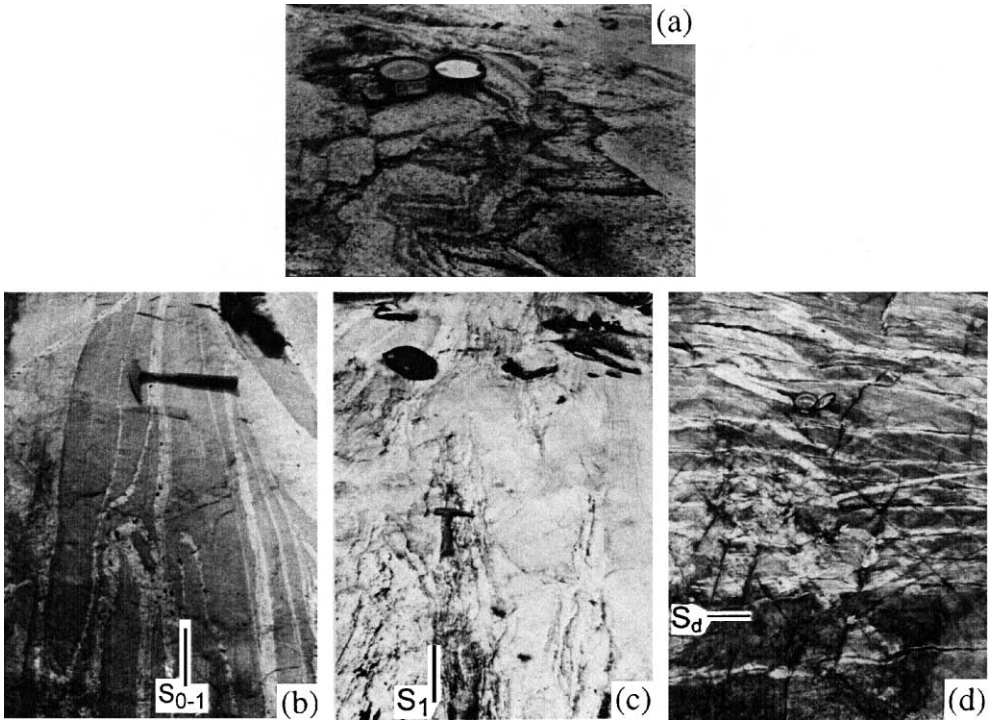

Fig. 5. Mesostructures in the Estrela Granite Complex: (a) horizontal S_0 foliation defined by alternating quartzofeldspathic and hornblende–biotite layers in pluton 2 (the L_1 lineation is visible on the right); (b) deformed pegmatite veins cross-cutting a monzogranite (grey) and displaying conformable (rectilinear, in a position of longitudinal joints) or oblique (folded, in a position of diagonal joints) relationships with the composite S_{0-1} surface which is faintly visible in the monzogranite (southern margin of pluton 3); (c) folded granitic dyke (to the right of the hammer) with the S_1 foliation axial planar for the folds (southern margin of pluton 1); (d) late EW-trending dissolution jointing (southern contact of pluton 3).

orientation (granoblastic textures), or may occur as aggregates of fine-grained polygonal neoblasts showing a more intense preferred orientation.

The minimum finite strain associated with S_1 has been estimated following Lapique et al. (1988) from axial ratios of feldspars and quartz grains, discarding the highly deformed and recrystallized rocks. Finite strain ellipsoid determination indicates that deformation was mainly flattening and subordinately plane deformation (Fig. 7) in agreement with the weakness of the lineation and the predominance of oblate tectonites ($S \gg L$). Only the southern part of the Estrela Granite Complex displays some constrictive components. Mylonitic bands, decimetre- to metre-wide and parallel to S_1, occur in plutons 2 and 3. A weak stretching lineation is locally observed ($S \gg L$ tectonites). Symmetrical conjugate shear zones are common, but, locally, strain shadows of amphibole porphyroclasts suggest a slight sinistral transcurrent movement. The stability of ferropargasite (Gilbert et al., 1982) suggests that these mylonites developed under high/medium temperature conditions.

4.2. Near-solidus to subsolidus microstructures and phase transformations

From above-solidus to sub-solidus low-temperature conditions, the following structures and mineral transformations are identified.

4.2.1. Conjugate small-scale shear bands

They occur in monzogranites displaying a well-developed S_1 foliation and intense intracrystalline deformation. These bands making an acute angle of 50° bisected by S_1 (Fig. 6b) are outlined by small unstrained crystals (~ 50 μm) of the same nature and composition as those from the host rocks (ferropargasite, feldspars and quartz), suggesting they may have

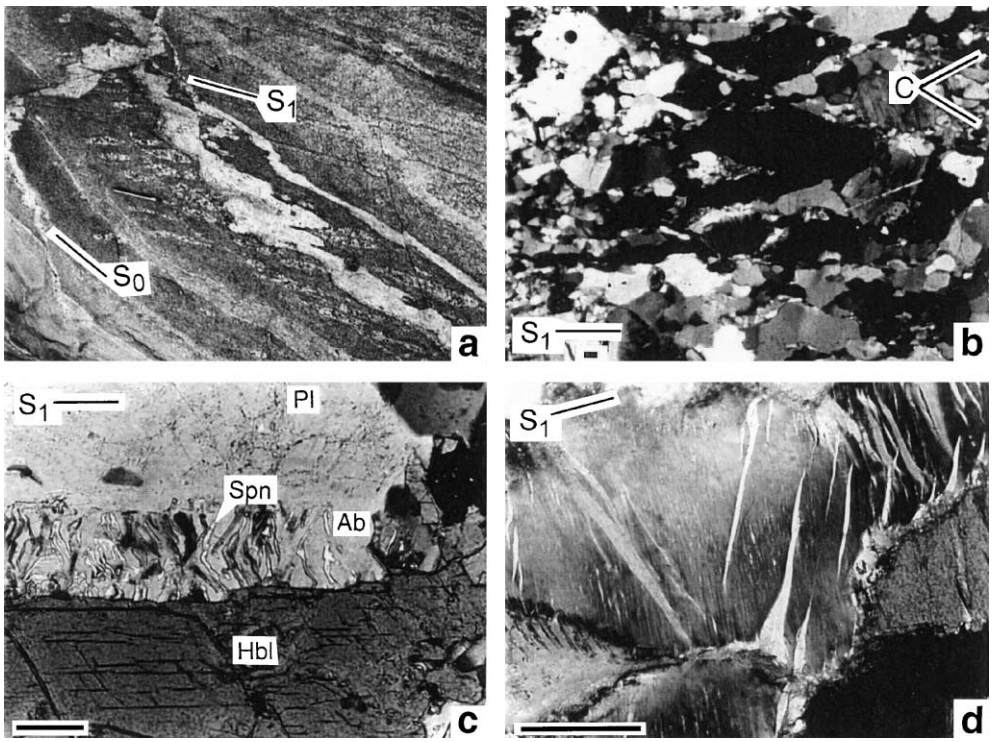

Fig. 6. Meso- and microstructures in the Estrela Granite Complex: (a) lenticular ilmenite-bearing leucocratic pods (close to the pencil) parallel to the S_1 foliation axial planar for the folds (pluton 2); (b) conjugate shear bands in monzogranites, outlined by fine-grained crystals of quartz, feldspar and amphibole (pluton 3); (c) albite–sphene symplectite developed at the expense of hornblende along a prismatic face (pluton 3); (d) conjugated flame perthites developed in a microperthite (the line bisecting the acute angle is perpendicular to S_1). Scale bar = 0.1 mm.

formed from the crystallization of residual melts collected in the shear bands (Bouchez et al., 1992).

4.2.2. The S_1 foliation

It is locally outlined by quartzofeldspathic pods containing ilmenite crystals that arose from the breakdown of biotite (Fig. 6a). Although they may be strongly flattened, no plastic deformation of minerals is observed, suggesting that both reaction and deformation occurred in the presence of a melt phase.

4.2.3. Subsolidus structures

In deformed monzogranites, hornblende is partly replaced by a symplectite consisting of sphene lamellae within an albite matrix (Fig. 6c). The symplectites developed between hornblende and feldspars, on the contact parallel to S_1, the sphene lamellae being grossly perpendicular to the foliation. They are as much abundant as monzogranites are deformed, suggesting that they grew at the expense of amphibole in relation with deformation. These textures are close to the myrmekitic textures reported by Simpson and Wintsch (1989) who consider that reactions leading to volume loss are favoured along crystals faces perpendicular to the maximum compressive stress. K-feldspars from monzogranites correspond commonly to a homogeneous microperthite, overprinted by coarse flame perthites, suggesting two stages of exsolution. Flame perthites display three preferred orientations (including in a same grain): lamellae perpendicular to S_1 (i.e. in a position of tension gash), and lamellae occurring as conjugated sets symmetrical with respect to S_1 (Fig. 6d). This suggests that growth of flame perthites is deformation controlled in agreement with previous observations (Debat et al., 1978; Brown and Parson, 1993; Pryer and Robin, 1996), and results from coaxial deformation. Low-grade joints associated with stilpnomelane–magnetite-bearing assemblages are lo-

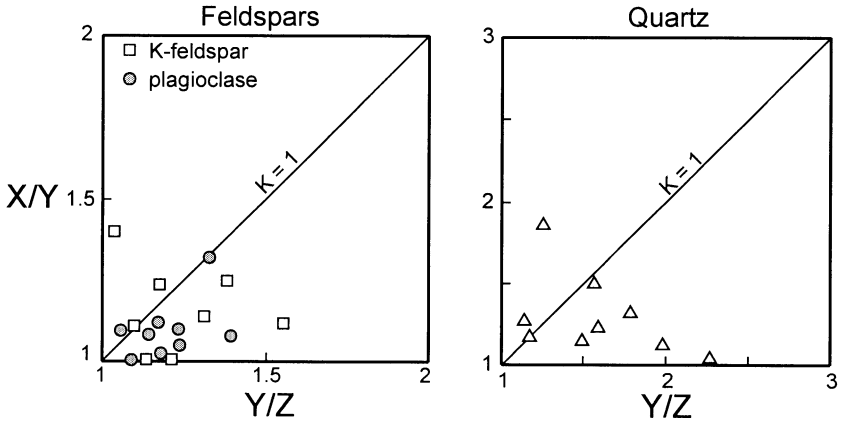

Fig. 7. Flinn plots for K-feldspar, plagioclase and quartz in samples from the Estrela Granite Complex. Most of the samples are below or on the line $K=1$ of plane strain and indicate a flattening strain ellipsoid.

cally observed (e.g. southern contact of pluton 3). They correspond to planes of intense dissolution leading to a closely spaced jointing (Fig. 5d).

4.2.4. Veins

Hydrothermal veins consisting of a hornblende rim and a quartz + albite core are observed mainly in the contact aureole. They occur dominantly as NS vertical veins and as both dextral and sinistral en echelon sets (NW–SE and NE–SW). This suggests a dominantly co-axial deformation with a shortening direction close to N10°E.

5. Discussion

The very low-grade metamorphic phase assemblages preserved in the Aguas Claras Formation, the presence of undeformed, 2.5- and 1.9-Ga, post-tectonic granites, along with preservation of the contact aureole and igneous textures in the surrounding greenstones clearly show that the Estrela Granite Complex did not suffer significant changes subsequently to its intrusion, and that its structures result from the dynamics of emplacement.

5.1. Conditions of emplacement and consolidation of the Estrela Granite Complex

The Estrela Granite Complex emplaced at a relatively shallow level ($P \leq 380$ MPa) in low-grade greenstones. Structures and deformation–recrystallization relationships lead this complex to be defined as synkinematic (e.g. Brun and Pons, 1981; Castro, 1987; Gapais, 1989; Paterson et al., 1989; Gower, 1993): (i) parallelism of foliation trajectories within the granites and the host greenstones; (ii) geometry of the banded iron formations to the east of the Estrela Granite Complex and triple junction foliation patterns in the host rocks at the terminations of plutons 1 and 2; (iii) progressive deformation under decreasing temperature, and presence within the granite massif of high-temperature mylonites; and (iv) growth of syntectonic garnet porphyroblasts in the contact aureole.

Microstructures perpendicular or symmetrical with respect to S_1 in both the granites and the contact aureole suggest mainly a co-axial deformation: (i) conjugate shear bands, (ii) flame perthites in feldspars, (iii) sphene–plagioclase symplectites in deformed monzogranites, (iii) subvertical high-T mylonites displaying C' symmetrical to S_1 (Berthé et al., 1979), and (iv) hydrothermal veins in both the xenoliths and host metabasites occurring as conjugated dextral and sinistral en echelon sets. Nevertheless, the presence of asymmetrical and rotational structures (sinistral) in the mylonites suggests a strike–slip component. This structural pattern is in agreement with the overall transpressional tectonic regime envisaged by Pinheiro and Holdsworth (1997) for the Carajás Province at the time of emplacement of the Estrela Granite Complex. This is also consistent with previous conclusions on the relationships between granite emplacement and

transpressional regimes (e.g. Gleizes et al., 1997, 1998). The *X* and *Z* axes of the bulk strain ellipsoid are near horizontal, and close to EW and NS for plutons 1 and 3, and close to N20°E and N110°E for pluton 2. The cause of this distinct pluton orientation is not fully clear, but it could be tentatively considered as a result of a local variation in the stress pattern due to the presence of important lithological heterogeneities (i.e. plutons 1 and 3). In this case, pluton 2 may have emplaced, subsequently to plutons 1 and 3, in a tension gash formed in relation with a sinistral strike–slip component (see Castro and Fernandez, 1998).

5.2. Magma pressure, tectonic stress, amount of crystallization and foliations

The first point to be emphasized is that emplacement and consolidation of the Estrela Granite Complex resulted from a continuous process, that is, that deformation started in the presence of a melt phase and ended under low-temperature subsolidus conditions. This is supported by the following data: (i) development of an igneous layering parallel to the pluton edges; (ii) emplacement of widespread synplutonic granite and pegmatite (aplite) dykes and veins corresponding to residual melts, associated with the development of S_1; (iii) flattening of ilmenite-bearing quartzofeldspathic pods outlining the S_1 surface without plastic deformation; and (iii) formation of high/medium-temperature mylonites, sphene–plagioclase symplectites, flame perthites and, lastly, of low-grade assemblages associated with dissolution joints. Therefore, we suggest that the finite deformation pattern corresponding to the succession of the two distinct types of structures, S_0 and S_1, should not be interpreted as distinct events, but simply as snapshots of a continuous evolution which reflect different amounts of crystallization (i.e. increasing crystal/melt ratio).

The first-formed foliation (S_0) defined by a rhythmic phase layering parallel to the limits of each of the three plutons implies crystal–liquid fractionation in response to cooling, and thus crystallization of possibly convecting magma chambers (e.g. Jaupart and Tait, 1995; Tait and Jaupart, 1996). At the microscopic scale, minerals are weakly deformed with medium-grained granoblastic textures and a weak quartz grain-shape fabric. This indicates that all these stages occurred under high-*T* magmatic conditions (pre-full crystallization fabric; Hutton, 1988) in a melt-dominated volume. Development of a rhythmic phase layering further suggests emplacement of crystal-poor, low-viscosity, magmas in agreement with the data of Scaillet et al. (1999, 2000). At this stage, the magma pressure overcame the total principal stress and led to lateral expansion of pluton and magma ponding. As shown (Clemens and Mawer, 1992; Hogan et al., 1998), this implies the existence of a horizontal strength anisotropy that acted as a magma trap (possibly the banded iron formations?).

The second-formed subvertical foliation (S_1), the subhorizontal lineation and the related structures reflect a horizontal shortening along the NS and an extension along the EW directions. This stage, associated with the emplacement of dykes of granite magma, and of fluid-enriched differentiated melts collected through deformation and concentrated in dilatant sites, indicates that the S_1 foliation developed initially in a highly crystallized mass under temperature conditions close to the granite solidus. Quartz deformation history and mineral transformations show that the subsequent deformation occurred in a fully crystallized medium under conditions extending down to low temperatures. The development of the S_1 foliation, corresponding to the stage of consolidation of the plutons (crystal plastic strain fabric; Hutton, 1988), appears to be controlled by the regional tectonic stress and suggests that the magma pressure was an insignificant parameter at that stage (except for local intrusion of granite bodies), due to the high amount of crystallization.

5.3. A possible succession of events during cooling of syntectonic plutons

The evolution of the plutons forming the Estrela Granite Complex, with development of two successive foliations and related structures, can be reconstructed in a single-stage process under decreasing temperatures. This can be accounted for in terms of both magma-driving pressure (Hogan et al., 1998) and crystallization progress. Although a pluton can be considered first as an expanding body, magma pressure is likely to become a less significant parameter with respect to the regional stress with ongoing crystallization, especially when the rigid percolation threshold is crossed (fraction of residual melt lower

than 0.5; Vigneresse et al., 1996). Here, if the strength of the crystallizing body is lower than the regional horizontal normal stress, as one can expect, pluton is likely to be strained with significant deformation of the phase layering and with segregation and redistribution of highly differentiated, fluid-enriched, residual melts. Therefore, we propose to split this evolution into the following two main periods.

(1) Magma emplacement is initially controlled by the magma pressure and the space occupied by the magma is accommodated by the host rocks. Inflation may have occurred from vertical sheeted bodies perpendicular to σ1 (EW-trending plutons 1 and 3), or in the position of a tension gash (NS-trending pluton 2), giving elliptical bodies (Fig. 8a) by alteration of the local stress field by magma intrusion (McCarthy and Thompson, 1988; Hogan and Gilbert, 1995; Vigneresse et al., 1999). However, even though the three plutons might be initiated by opening of a fracture as proposed by Castro and Fernandez (1998), they are forceful intrusions as shown by the significant deformation of the country rocks. As long as plutons are melt dominated, magma pressure remains the dominant parameter and almost no tectonic strain is recorded. Magmas ponded differentiate by fractional crystallization leading to the development of a phase layering (S_0; Fig. 8b), grossly parallel to the limits of the plutons as crystallization is controlled by heat removal and proceeds from the walls by progression of the crystallization front and onset of convection (e.g. Tait and Jaupart,

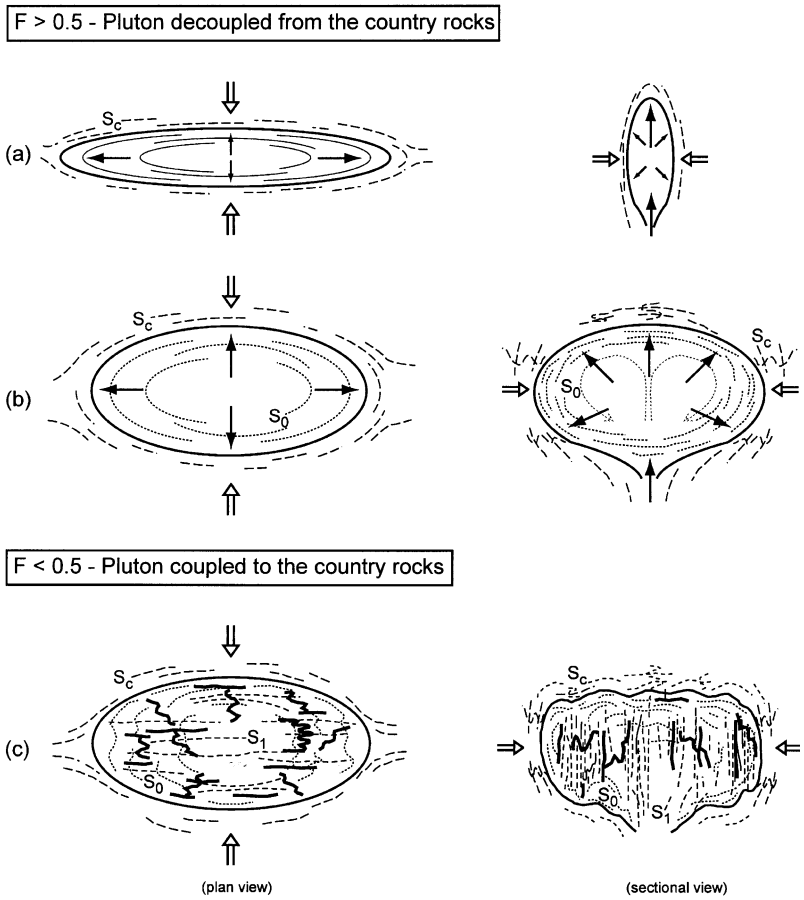

Fig. 8. Synopsis of the evolution of the Estrela Granite Complex (plan and sectional views). The regional constraint is supposed to be constant during emplacement and consolidation. See text for further explanation. Bold lines represent pegmatite and granite dykes and veins. *F* = residual melt fraction.

1996; Irvine and Andersen, 1998). The S_0 foliation thus reflects the period of magma differentiation. The early layering may have been subsequently flattened circumferentially by injection of successive magma batches (see, for example, Ramsay, 1989), accounting for the grain-shape fabric parallel to S_0. As long as the rheology is melt dominated, the magma pressure remains a significant parameter, even though the whole process is likely to be tectonically driven. This main period of pluton construction is characterized by a high degree of mechanical decoupling of the growing magmatic body to its country rocks, and depends dominantly on internal magma chamber processes (Paterson et al., 1998).

(2) For high amounts of crystallization, that is, crystal proportions higher than the rigid percolation threshold, a rigid crystal framework is established, the magma pressure becomes insignificant (except for local melt redistribution), and the whole crystallized mass becomes coupled to the host rocks and starts deforming. Hence, the subsequent evolution is controlled by the regional tectonics, because the total principal stress exceeds the strength of the pluton. This leads to the deformation of the partially crystallized magmatic volume (deformation of the primary layering, crystal sorting by mechanical segregation, etc.), redistribution of the residual melts by strain localization within shear fractures (e.g. Rosenberg and Handy, 2000), and development of a near-solidus to subsolidus fabric (S_1; Fig. 8c). The largest amount of strain is likely to be recorded during this period, as it spreads from above-solidus conditions down to low-grade conditions. This is the period during which plutons become completely coupled to the country rocks (Paterson et al., 1998).

6. Conclusion

In conclusion, the emplacement and consolidation of the three plutons forming the Estrela Granite Complex appears to result from a continuous evolution under decreasing temperatures in a single-stage, strained crust (transpression). The whole evolution of the plutons appears to have been controlled first by the magma pressure and flow, and then by the tectonic stress and solid state deformation, the transition being related to the amount of crystallization through the rheological transitions, by coupling of plutons with their surrounding deforming crust. The first period controlled by body forces appears as a period during which pluton behaves as a composite magma chamber that differentiates by fractional crystallization. Most of the strain is recorded subsequently during the second period controlled by tectonic forces, when the crystal fraction exceeds the rigid percolation threshold.

Acknowledgements

Thanks to R. Dall'Agnol, J. Pons, G. Gleizes and J.L. Vigneresse for stimulating discussions and comments on the manuscript. We gratefully acknowledge the detailed reviews by A. Castro and J.P. Hogan which helped us to express our view more clearly. Financial support from the Conselho Nacional de Desenvolvimento Científico e Technológico (Grant 200774/93-0 to C.E.M.B.), Universidade Federal do Pará (Centro de Geociências, Belém), Université Henri Poincaré (JE-239) and Centre de Recherches Pétrographiques et Géochimiques (CNRS), is gratefully acknowledged. CPRG contribution no. 1512.

References

Almeida, F.F.M., Hasui, Y., Brito-Neves, B.B., Fuck, R.A., 1981. Brazilian structural provinces: an introduction. Earth Sci. Rev. 17, 1–29.

Althoff, F.J., Barbey, P., Boullier, A.M., 2000. 2.8–3.0 Ga plutonism and deformation in the SE Amazonian craton. The Archaean granitoids of Marajoara (Carajás Mineral Province, Brazil). Precambrian Res. 104, 187–206.

Anderson, J.L., Smith, D.R., 1995. The effects of temperature and f_{O2} on the Al-in-hornblende barometer. Am. Mineral. 80, 549–559.

Andrade, J.B.F., 1991. Folha SB.22-Z-A. Estado do Pará. Texto Explicativo. In: Araújo, O.J.B., Maia, R.G.N. (Eds.), Programa Levantamentos Geológicos Básicos do Brasil, Programa Grande Carajás, Serra dos Carajás. DNPM/CPRM, Brasília, pp. 69–77.

Araújo, O.J.B., Maia, R.G.N., Jorge-João, X.S., Costa, J.B.S., 1988. A Megaestruturação Arqueana da Folha Serra dos Carajás, 7th Congr. Latino-Am. Geol., Belém, Anais, SBG, Sao Paulo, vol. 1, 324–338.

Arzi, A.A., 1978. Critical phenomena in the rheology of partially melted rocks. Tectonophysics 44, 173–184.

Avelar, V.G., 1996. Geochronologia Pb–Pb, por evaporação em monocristal de zircão, do magmatismo de região de Tucumá, SE do Estado do Pará, Amazonia Oriental. Master thesis, Univ. Federal do Pará, Belèm.

Baer, G., Reches, Z., 1991. Mechanisms of emplacement and tec-

tonic implications of the Ramon dike systems, Israel. J. Geophys. Res. 96, 11895–11910.
Balk, R., 1937. Structural behaviour of igneous rock. Geol. Soc. Am. Mem. 5, 1–77.
Barrière, M., 1981. On curved laminae, graded layers, convection currents and dynamic crystal sorting in the Ploumanac'h (Brittany) subalkaline granite. Contrib. Mineral. Petrol. 77, 214–224.
Barrière, M., Cotten, J., 1979. Biotites and associated minerals as markers of magmatic fractionation and deuteric equilibration in granites. Contrib. Mineral. Petrol. 72, 183–192.
Barros, C.E.M., Dall'Agnol, R., Lafon, J.M., Teixeira, N.P., Ribeiro, J.W., 1992. Geologia e geocronologia Rb–Sr do Gnaisse Estrela, Curionópolis, PA. Bol. Mus. Para. Emílio Goeldi, Ciênc. da Terra 4, 83–104.
Barros, C.E.M., Dall'Agnol, R., Barbey, P., Boullier, A.M., 1997. Geochemistry of the Estrela Granite Complex, Carajás Region, Brazil: an example of an Archaean A-type granitoid. J. S. Am. Earth Sci. 10, 321–330.
Barros, C.E.M., Macambira, M.J.B., Barbey, P., 2001. Idade de zircões do Complexo Granítico Estrela, Província Metalogenética de Carajás, Brazil. In: VIII Congr. Brazil. Geoquimica, SBG, Sao Paulo, pp. 67–68.
Berthé, D., Choukroune, P., Jegouzo, P., 1979. Orthogneiss, mylonites and non-coaxial deformation of granites: the example of the South Armorican shear zone. J. Struct. Geol. 1, 31–42.
Bouchez, J.L., Delas, C., Gleizes, G., Nédélec, A., Cuney, M., 1992. Submagmatic microfractures in granites. Geology 20, 35–38.
Brandeis, G., Marsh, B.D., 1989. The convective liquidus in a solidifying magma chamber: a fluid dynamic investigation. Nature 339, 613–616.
Brown, W.L., Parson, I., 1993. Storage and release of elastic strain energy: the driving force for low-temperature reactivity and alteration of alkali feldspar. In: Boland, J.N., Fitz, G. (Eds.), Defects and Processes in the Solid State: Geoscience Applications (the McLaren volume) Dev. Petrol. 2, pp. 281–287.
Brun, J.P., Pons, J., 1981. Strain patterns emplacement in a crust undergoing non-coaxial deformation, Sierra Morena, Southern Spain. J. Struct. Geol. 3, 219–229.
Castro, A., 1987. On granitoid emplacement and related structures. A review. Geol. Rundsch. 6, 101–124.
Castro, A., Fernandez, C., 1998. Granite intrusion by externally induced growth and deformation of the magma reservoir, the example of the Plasenzuela pluton, Spain. J. Struct. Geol. 20, 1219–1228.
Clarke, D.B., Clarke, G.K.C., 1998. Layered granodiorites at Chebucto Head, South Mountain batholith, Nova Scotia. J. Struct. Geol. 20, 1305–1324.
Clemens, J.D., Mawer, C.K., 1992. Granitic magma transport by fracture propagation. Tectonophysics 204, 339–360.
Clemens, J.D., Holloway, J.R., White, A.J.R., 1986. Origin of an A-type granite: experimental constraints. Am. Mineral. 71, 317–324.
Collins, W.J., Beams, S.D., White, A.J.R., Chappell, B.W., 1982. Nature and origin of A-type granites with particular reference to southeastern Australia. Contrib. Mineral. Petrol. 80, 189–200.
Creaser, R.A., Price, R.C., Wormald, R.J., 1991. A-type granites revisited: assessment of a residual-source model. Geology 19, 163–166.
Czamanske, G.K., Wones, D.R., 1973. Oxidation during magmatic differentiation, Finnmarka Complex, Oslo area, Norway: Part 2. The mafic silicates. J. Petrol. 14, 349–380.
Dall'Agnol, R., Lafon, J.M., Macambira, M.J.B., 1994. Proterozoic anorogenic magmatism in the Central Amazonian Province, Amazonian Craton: geochronological, petrological and geochemical aspects. Mineral. Petrol. 50, 113–138.
Davidson, C., Schmid, S.M., Hollister, L.S., 1994. Role of melt during deformation in the deep crust. Terra Nova 6, 133–142.
Debat, P., Soula, J.C., Kubin, L., Vidal, J.L., 1978. Optical studies of natural deformation microstructures in feldspars (gneiss and pegmatites from Occitania, southern France). Lithos 11, 133–145.
Dias, G.S., Macambira, M.J.B., Dall'Agnol, R., Soares, A.D.V., Barros, C.E.M., 1996. Datação de zircões de sill de metagabros: comprovação da idade arqueana da Formação águas Claras, Carajás—Pará. 5th Simp. Geol. Amaz., Extended abstracts. SBG, Belém, pp. 376–379.
Docegeo, 1988. Revisão litoestratigráfica de província mineral de Carajás. Província Mineral de Carajás—Litoestratigrafia e principais depósitos minerais, 35th Congr. Bras. Geol., Anexo Anais. CVRD/SBG, Belém, pp. 11–59.
Eby, G.N., 1990. The A-type granitoids: a review of their occurrence and chemical characteristics and speculations on their petrogenesis. Lithos 26, 115–134.
Eby, G.N., 1992. Chemical subdivision of the A-type granitoids: petrogenesis and tectonic implications. Geology 20, 641–644.
Eugster, H.P., Wones, D.R., 1962. Stability relations of the ferruginous biotite, annite. J. Petrol. 3, 82–125.
Ferry, J.M., Spear, F.S., 1978. Experimental calibration of the partitioning of Fe and Mg between biotite and garnet. Contrib. Mineral. Petrol. 66, 113–117.
Gapais, D., 1989. Les orthogneiss—structures, mécanismes de déformation et analyse cinématique. Mém. Doc. Centre Armoricain Et. Struct., vol. 28. Socles, Rennes, 366 pp.
Gilbert, M.C., 1966. Synthesis and stability relations of the hornblende ferropargasite. Am. J. Sci. 264, 698–742.
Gilbert, M.C., Helz, R.T., Popp, R.K., Spear, F.S., 1982. Experimental studies of amphibole stability. In: Veblen, D.R., Ribbe, P.H. (Eds.), Amphiboles: Petrology and Experimental Phase Relations. Mineral. Soc. Am., Rev. Mineral. 9B, pp. 229–353.
Gleizes, G., Leblanc, D., Bouchez, J.L., 1997. Variscan granites of the Pyrenees revisited: their role as syntectonic markers of the orogen. Terra Nova 9, 38–41.
Gleizes, G., Leblanc, D., Santana, V., Olivier, P., Bouchez, J.L., 1998. Sigmoidal structures featuring dextral shear during emplacement of the Hercynian granite complex of Cauterets–Panticosa (Pyrenees). J. Struct. Geol. 20, 1229–1245.
Gower, C.F., 1993. Syntectonic minor intrusions or synemplacement deformation? Can. J. Earth Sci. 30, 1674–1675.
Graham, C.M., Powell, R., 1984. A garnet–hornblende geothermometer: calibration, testing and application to the Pelona Schist, Southern California. J. Metamorph. Geol. 2, 13–31.
Harrison, T.M., Watson, E.B., 1984. The behavior of apatite during

crustal anatexis: equilibrium and kinetic considerations. Geochim. Cosmochim. Acta 48, 1467–1477.

Hirata, W.K., Rigon, J.C., Kadekaru, K., Cordeiro, A.A.C., Meireles, E.M., 1982. Geologia Regional da Província Mineral de Carajás, 1st Simp. Geol. Amaz., Anais, vol. 1. SBG, Belém, pp. 100–110.

Hogan, J.P., Gilbert, M.C., 1995. The A-type Mount Scott Granite sheet: importance of crustal magma trap. J. Geophys. Res. 100, 15779–15793.

Hogan, J.P., Price, J.D., Gilbert, M.C., 1998. Magma traps and driving pressure: consequences for pluton shape and emplacement in an extensional regime. J. Struct. Geol. 20, 1155–1168.

Huhn, S.R.B., Macambira, M.J.B., Dall'Agnol, R., 1999. Geologia e geochronologia Pb/Pb do granito alcalino Planalto, região da Serra do Rabo, Carajás, P.A., VI Simp. Geol. Amazônia, Manaus, 463–466.

Hutton, D.H.W., 1988. Granite emplacement mechanisms and tectonic controls: inferences from deformation studies. Trans. R. Soc. Edinburgh: Earth Sci. 79, 245–255.

Hutton, D.H.W., 1997. Syntectonic granites and the principle of effective principal stress: a general solution to the space problem? In: Bouchez, J.L., Hutton, D.H.W., Stephen, W.E. (Eds.), Granite: From Segregation of Melt to Emplacement Fabrics. Kluwer Academic Publishers, Dordrecht, pp. 189–197.

Irvine, T.N., Andersen, J.C.Ø., 1998. Included blocks (and blocks within blocks) in the Skaergaard intrusion: geologic relations and the origins of rhythmic modally graded layers. Geol. Soc. Am. Bull. 110, 1398–1447.

Jaupart, C., Tait, S., 1995. Dynamics of differentiation in magma reservoirs. J. Geophys. Res. 100, 17615–17636.

Kretz, R., 1983. Symbols for rocks-forming minerals. Am. Mineral. 68, 277–279.

Kuniyoshi, S., Liou, J.G., 1976. Contact metamorphism of the Karmutsen volcanics, Vancouver Island, British Columbia. J. Petrol. 17, 73–99.

Kurshakova, L.D., Avetisyan, E.I., 1974. Stability and properties of synthetic hedenbergite. Geochim. Int. 3, 338–346.

Laird, J., 1988. Chlorites: metamorphic petrology. In: Bailey, S.W. (Ed.), Hydrous Phyllosilicates (Exclusive of Micas). Mineral. Soc. Am., Rev. Mineral. 19, pp. 405–453.

Lapique, F., Champenois, M., Cheilletz, A., 1988. Un analyseur vidéographique interactif: dévelopment et applications. Bull. Minéral. 111, 679–687.

Loiselle, M.C., Wones, D.R., 1979. Characteristics of anorogenic granites. Geol. Soc. Am. 11, 468. Abstracts with Programs.

Macambira, M.J.B., Lafon, J.M., 1995. Geocronologia da Província Mineral de Carajás; síntese dos dados e novos desafios. Bol. Mus. Para. Emílio Goeldi, Cienc. da Terra 7, 263–288.

Machado, N., Lindenmayer, Z., Krogh, T.H., Lindenmayer, D., 1991. U–Pb geochronology of Archaean magmatism and basement reactivation in the Carajás area, Amazon shield, Brazil. Precambrian Res. 49, 329–354.

Marre, J., 1986. The Structural Analysis of Granitic Rocks. Elsevier, New York.

McCarthy, J., Thompson, G.A., 1988. Seismic imaging of extended crust with emphasis on the western United States. Geol. Soc. Am. Bull. 100, 1361–1374.

Miller, R.B., Paterson, S.R., 1994. The transition from magmatic to high-temperature solid-state deformation: implications from the Mount Stuart Batholith, Washington. J. Struct. Geol. 16, 853–865.

Mougeot, R., 1996. Etude de la limite Archéen-Protérozoique et des minéralisations Au, +/−U associées. Exemples de la région de Jacobina (Etat de Bahia, Brésil) et de Carajás (Etat de Para, Brésil). Unpubl. thesis, University of Montpellier II, 301 pp.

Olszewski, W.J., Wirth, K.R., Gibbs, A.K., Gaudette, H.E., 1989. The age, origin and tectonics of the Grão Pará group and associated rocks, Serra dos Carajás, Brazil. Precambrian Res. 42, 229–254.

Parsons, T., Sleep, N.H., Thompson, G.A., 1992. Host rock rheology controls on the emplacement of tabular intrusions: implications for underplating of extending crust. Tectonics 11, 1348–1356.

Paterson, S.R., Vernon, R.H., Fowler Jr., T.K., 1989. Aureole systematics. In: Ribbe, P.H. (Ed.), Contact Metamorphism. Mineral. Soc. Am., Rev. Mineral. vol. 26, pp. 673–722.

Paterson, S.R., Fowler Jr., T.K., Schmidt, K.L., Yoshinobu, A.S., Yuan, E.S., Miller, R.B., 1998. Interpreting magmatic fabric patterns in plutons. Lithos 44, 53–82.

Patiño Douce, A.E., 1997. Generation of metaluminous A-type granites by low-pressure melting of calc-alkaline granitoids. Geology 25, 743–746.

Pinheiro, R.V.L., Holdsworth, R.E., 1997. Reactivation of Archaean strike–slip fault systems, Amazon region, Brazil. J. Geol. Soc. (London) 154, 99–103.

Pons, J., Barbey, P., Dupuis, D., Léger, J.M., 1995. Mechanism of pluton emplacement and structural evolution of a 2.1 Ga juvenile continental crust: the Birimian of southwestern Niger. Precambrian Res. 70, 281–301.

Pryer, L.L., Robin, P.Y.F., 1996. Differential stress control on the growth and orientation of flame perthite: a paleostress-direction indicator. J. Struct. Geol. 18, 1151–1166.

Ramsay, J.G., 1989. Emplacement kinematics of a granite diapir: the Chindamora batholith, Zimbabwe. J. Struct. Geol. 2, 191–209.

Rodrigues, E.S., Lafon, J.M., Scheller, T., 1992. Geocronologia Pb–Pb da Província Mineral de Carajás: primeiros resultados, 37th Congr. Bras. Geol. 2, Extended abstracts. SBG, São Paulo, pp. 183–184.

Roman-Berdiel, T., Gapais, D., Brun, J.P., 1995. Analogue models of laccolith formation. J. Struct. Geol. 17, 1337–1346.

Rosenberg, C.L., Handy, M.R., 2000. Syntectonic melt pathways during simple shearing of a partially molten rock analogue (Norcamphor–Benzamide). J. Geophys. Res. 105, 3135–3149.

Scaillet, B., Holtz, F., Whittington, A., Pichavant, M., 1999. The viscosity of silicic magmas: a review from the viewpoint of experimental petrology. In: Barbarian, B. (Ed.), The Origin of Granites and Related Rocks, IVth Hutton Symposium, vol. 290 Doc. BRGM, Orléans, p. 111. Abstract.

Scaillet, B., Whittington, A., Martel, C., Pichavant, M., Holtz, F., 2000. Phase equilibrium constraints on the viscosity of silicic magmas: II. Implications for mafic–silicic mixing processes. Trans. R. Soc. Edinburgh: Earth Sci. 91, 61–72.

Schofield, D.L., D'Lemos, R.S., 1998. Relationships between syn-

tectonic granite fabrics and regional PTtd paths: an example from the Gander–Avalon boundary of NE Newfoundland. J. Struct. Geol. 20, 459–471.

Simpson, C., Wintsch, R.P., 1989. Evidence for deformation-induced K-feldspar replacement by myrmekite. J. Metamorph. Geol. 7, 261–275.

Souza, Z.S., Dall'Agnol, R., Althoff, F.J., Leite, A.A.S., Barros, C.E.M., 1996. Carajás Mineral Province: geological, geochronological and tectonic contrasts on the Archean evolution of the Rio Maria granite–greenstone terranes and the Carajás Block, Symposium Archaean Terranes of the South American Platform, Extended abstracts. SBG, Brasília, pp. 31–32.

Spear, F.S., 1993. Metamorphic Phase Equilibria and Pressure–Temperature–Time Paths. Mineral. Soc. Am., Washington Monograph, 799 p.

Stephenson, P.J., 1990. Layering in felsic granites in the main East pluton, Hinchinbrook Island, North Queensland, Australia. Geol. J. 25, 325–336.

Tait, S., Jaupart, C., 1996. The production of chemically stratified and accumulate plutonic igneous rocks. Mineral. Mag. 60, 99–114.

Trendall, A.F., Basei, M.A.S., De Laeter, J.R., Nelson, D.R., 1998. SHRIMP zircon U–Pb constraints on the age of the Carajás formation, Grão Pará Group, Amazon craton. J. S. Am. Earth Sci. 11, 265–277.

Tribe, I.R., D'Lemos, R.S., 1996. Significance of hiatus in decreasing-temperature fabric development within syn-tectonic quartz diorite complexes, Channel Island, U.K. J. Geol. Soc. 153, 127–138.

Van der Molen, I., Paterson, M.S., 1979. Experimental deformation of partially-melted granite. Contrib. Mineral. Petrol. 70, 299–318.

Vigneresse, J.L., Clemens, J.D., 2000. Granitic magma ascent and emplacement: neither diapirism nor neutral buoyancy. In: Vendeville, B., Mart, Y., Vigneresse, J.L. (Eds.), Salt Shale and Igneous Diapirs in and around Europe. Geol. Soc., London, Spec. Publ. 174, pp. 1–19.

Vigneresse, J.L., Barbey, P., Cuney, M., 1996. Rheological transitions during partial melting and crystallization with application to felsic magma segregation and transfer. J. Petrol. 37, 1579–1600.

Vigneresse, J.L., Tikoff, B., Améglio, L., 1999. Modification of the regional stress field by magma intrusion and formation of tabular granitic plutons. Tectonophysics 302, 203–224.

Watson, E.B., Harrison, T.M., 1983. Zircon saturation revisited: temperature and composition effects in a variety of crustal magma types. Earth Planet. Sci. Lett. 64, 295–304.

Whalen, J.B., Currie, K.L., Chappell, B.W., 1987. A-type granites: geochemical characteristics, discrimination and petrogenesis. Contrib. Mineral. Petrol. 95, 407–419.

Wickham, S.M., 1987. The segregation and emplacement of granitic magmas. J. Geol. Soc. (London) 144, 281–297.

Wones, D.R., 1989. Significance of the assemblage titanite + magnetite + quartz in granitic rocks. Am. Mineral. 74, 744–749.

Wones, D.R., Gilbert, M.C., 1982. Amphiboles in the igneous environment. In: Veblen, D.R., Ribbe, P.H. (Eds.), Amphiboles: Petrology and Experimental Phase Relations. Mineral. Soc. Am., Rev. Mineral. 9B, pp. 355–389.